Numerical analysis of turbulent flame enhancement by nanosecond repetitively pulsed plasma discharges

Yacine Bechane, Benoit Fiorina

Numerical analysis of turbulent flame enhancement by nanosecond repetitively pulsed plasma discharges

Yacine Bechane [a,*] and Benoît Fiorina [a]

[a] *Université Paris-Saclay, CNRS, CentraleSupélec, Laboratoire EM2C, 91190, Gif-sur-Yvette, France*

Abstract

Experimental studies of plasma-assisted combustion have shown that Nanosecond Repetitively Pulsed (NRP) discharges are a very efficient way to improve flame stability in lean regimes. These discharges generate a non-equilibrium plasma that induces a local heating and an important production of active species sufficient to enhance the combustion. The aim of this article is to understand the physical and chemical mechanisms involved in plasma-assisted turbulent combustion. High-performance computations of a lean bluff-body turbulent premixed methane-air flame, experimented at EM2C laboratory, are conducted for that purpose. Simulations are performed by combining a semi-empirical plasma model with an analytical combustion mechanism. Without electrical discharges, only a weak reaction zone behind the bluff body is observed. However, when the flame is assisted with the plasma, the flame power and surface increase significantly. A chemical analysis performed at the flame basis shows that the heat and the radical O produced by NRP discharges induce the dissociation of main burnt gases species H_2O and CO_2 into radicals OH, H, CO, O and species H_2, O_2. The species with long lifespan OH, H_2 and O_2 are convected from the center of the bluff-body recirculation zone to the flame front where they are consumed increasing the chemical reactivity. This causes a local increase of heat release rate that attaches the turbulent flame front which can develop downstream.

Keywords: Plasma-assisted combustion; Nanosecond Repetitively Pulsed discharges; Turbulent premixed flame; Lean flame enhancement; Large Eddy Simulation

1. Introduction

The low temperature of lean flames prevents the NO_x production but may induce incomplete combustion, instabilities and extinctions [1].

An emerging solution to enable flame stabilization, suitable to a wide range of combustion applications, is to locally generate a plasma [2, 3]. Among the various possible types of discharges to enhance combustion [4, 5], the Nanosecond Repetitively Pulsed (NRP) discharges [6] succeeded to stabilize ultra-lean premixed flames on several laboratory-scale hydrocarbon-air flames [6, 7] but also in test rigs representative of a gas turbine environment at atmospheric [8, 9] and high pressure [10, 11]. This technique is very efficient because the energy consumption of the plasma is typically less than 1% of the power released by the flame.

The principle of flame stabilization by NRP discharges is illustrated in Fig. 1. NRP discharges are generated by applying a high voltage pulse (about 10kV) during approximatly 10 ns between two electrodes at a repetition frequency of the order of 10kHz. The NRP discharges cause first, at the nanosecond scale, an ultrafast increase of gas temperature and species dissociation [12]. This is followed by a slower gas heating process, appearing at the millisecond scale, induced by the relaxation of the nitrogen molecule's vibrational states. It has been shown experimentally [12] and numerically [13] that about 35% of the discharge energy dissociates up to 50% of the oxygen molecules contained in the inter-electrode region in O atoms. While it has been observed empirically that the NRP discharge is efficient when located in small gases recirculation zone, the fundamental mechanisms of plasma-assisted flame stabilization are not yet well understood. In particular, the physical and chemical processes that relate the O atom production to the heat release enhancement in a turbulent flame has not been completely identified.

High-performance computing is an attractive way to understand and explain such complex fundamental mechanisms. Very few CFD simulations have been however carried out to understand the influence of NRP discharges on the flame structure. Bak *et al.* [14] have simulated the plasma-assisted stabilization of a laminar methane/air flame by simultaneously solving the equations describing the discharge, the plasma, the flow, and the combustion kinetics. A similar computational strategy has been followed by Tholin *et al.* [15] to simulate the ignition of preheated quiescent H2/air mixtures excited by NRP discharges. While giving interesting insights into the impact of plasma on combustion, detailed simulations have been limited to 1-D and 2-D simulations in laminar flow conditions, because of their high computational cost. Computational domains have been also restricted to the plasma discharge vicinity, which is not sufficient to capture the large scales involved in a turbulent combustion chamber. Detailed simulations of plasma kinetics is today still too expensive to be directly included in 3-D turbulent flame simulations.

An alternative has been proposed by Castela *et al.* [16] to reduce the computational cost of the description of the complex plasma kinetic processes by using a phenomenological model which captures the main impacts of NRP on the combustion: the local increase of temperature and the oxygen dissociation [16]. Only one balance equation for the vibrational energy is added to the standard reactive flow balance equations, therefore the increase of CPU cost is limited. This approach has been succesfully applied to compute the ignition of flame kernel by NRP discharges [17]. This model has also been recently implemented in a Large Eddy Simulation (LES) flow solver to study the ignition sequence of a flame by a series of NRP discharges [18].

The objectives of this study are to give new insights into the plasma flame interaction mechanisms through the numerical analysis of the LES of plasma-assisted turbulent combustion. Section 2 presents the phenomenological plasma-assisted turbulent combustion model adapted with the LES formalism, while Section 3 gives details on the experimental configuration, called Mini-PAC, retained for performing the numerical investigation. Results are presented and analyzed in Sec.4 .

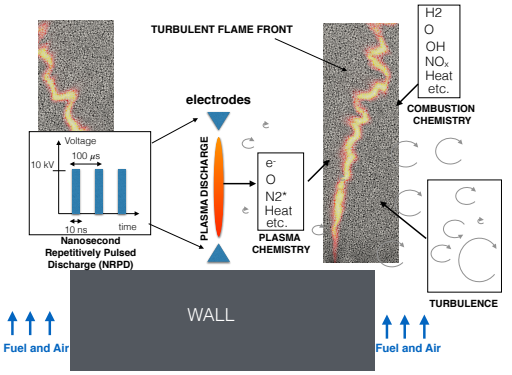

Fig. 1: Schematic view of major physical phenomena involved in plasma-assisted combustion. A nanosecond (repetitively pulsed) discharge generates a plasma in the vicinity of a flame. Heat and dissociated species (such as the radical O) interact with the flame front which is wrinkled by turbulence.

2. Modeling plasma-assisted turbulent combustion

2.1. Nanoseconds pulsed discharges model

The experimental [12] and numerical [13] studies of NRP discharges applied in pure air or lean fresh hydrocarbon-air mixtures showed that the discharge pulses mainly induce electronic and vibrational excitation of nitrogen molecules N_2. The nanosecond scale relaxation of the produced electronic states N_2(A,B,C,a', . . .) by dissociative quenching

with O_2 molecules leads leads to an ultra-fast increase of gas temperature and O_2 dissociation into atomic oxygen [12].The Relaxation of vibrational states of N_2 occurs on a much longer times scales, milliseconds scales, and results in slow gas heating. The recent measurement performed by Minesi *et al*. [19] showed that when applied in a mixture of lean flame burnt gases the NRP discharges induce similar effects.

Based on these observations, Castela *et al*. [16] developed a semi-empirical model that captures the effects of NRP dischrages on combustion without solving the electric field and the detailed plasma chemistry. Ultra-fast and slow processes are modeled by splitting into three contributions the rate of energy $\dot{E}^p$ deposited at each electrical discharge :

$$\dot{E}^p = \dot{E}^p_{chem} + \dot{E}^p_{heat} + \dot{E}^p_{vib} \tag{1}$$

The chemical $\dot{E}^p_{chem}$ and thermal $\dot{E}^p_{heat}$ contributions refer to the amount of energy transferred into the ultra-fast dissociation of species and gas heating, respectively. $\dot{E}^p_{vib}$ is the rate of energy transferred to vibrational state N_2. The model considers that only O_2 is dissociated by the discharge into atomic O. The energy contributions are modeled as [16]:

$$\dot{E}^p_{chem} = \eta \, \frac{Y_{O_2}}{Y^f_{O_2}} \, (1 - \frac{e_{O_2}}{e_O}) \, \dot{E}^p \tag{2}$$

$$\dot{E}^p_{heat} = [\alpha - \eta \, \frac{Y_{O_2}}{Y^f_{O_2}} \, (1 - \frac{e_{O_2}}{e_O})] \, \dot{E}^p \tag{3}$$

$$\dot{E}_{vib} = (1 - \alpha) \, \dot{E}^p \tag{4}$$

where $Y^f_{O_2}$ is the mass fraction of O_2 in the fresh mixture. e_k is the internal energy of species in mass units. α is the fraction of pulse energy that induces the electronic excitation of N_2 and subsequently the ultra-fast gas heating and ultra fast O_2 dissociation. η is the fraction of pulse energy that leads to O_2 dissociation, α - η the fraction that goes into ultra-fast heating and finally (1 - α) the remainings fraction that goes into the slow heating.

According to [19], the fraction of energy α responsible of the ultra-fast heating and the ultra-fast dissociation of species when NRP discharges are applied in lean burnt gases is similar to what was obtained for NRP discharges in pure air [12]. The fraction of energy that goes into ultra-fast heating (α - η) is also the same and is equal to 20%. Therefore, the parameters are here set to $\alpha = 55\%$ and $\eta = 35\%$.

2.2. LES balance equations

The LES reactive flow governing equations are combined with the Thickened Flame model for LES (TFLES) [20], which artificially thicken the reactive layer to avoid under-resolution issues of the flame front. In addition to the mass and momentum equations, the following balance equations are solved for total energy e, vibrational energy e_{vib} and species mass fractions Y_k:

$$\frac{\partial \overline{\rho}\widetilde{e}}{\partial t} + \frac{\partial (\overline{\rho}\widetilde{u_i}\widetilde{e})}{\partial x_i} = \frac{\partial}{\partial x_i}\left(C_p \left[F\Xi \frac{\mu}{P_r} + (1-S)\frac{\mu_t}{P^t_r}\right]\frac{\partial \widetilde{T}}{\partial x_i}\right) + \frac{\partial}{\partial x_i}\left(\sum_{k=1}^{N}\left[F\Xi \frac{\mu}{S_{c,k}} + (1-S)\frac{\mu_t}{S^t_{c,k}}\right]\frac{\partial \widetilde{Y_k}}{\partial x_i}\widetilde{h}_{s,k}\right) + \frac{\partial (\overline{\sigma_{ij}u_i})}{\partial x_i} \; + \; \overline{\dot{E}}^p_{chem} \; + \; \overline{\dot{E}}^p_{heat} \; + \; \overline{\dot{R}}^p_{VT} \tag{5}$$

$$\frac{\partial \overline{\rho}\widetilde{e}_{vib}}{\partial t} + \frac{\partial (\overline{\rho}\widetilde{u_i}\widetilde{e}_{vib})}{\partial x_i} = \frac{\partial}{\partial x_i}\left(\left[\frac{\overline{\mu}}{S_{c,evib}} + \frac{\mu_t}{S^t_{c,evib}}\right]\frac{\partial \widetilde{e}_{vib}}{\partial x_i}\right) + \overline{\dot{E}}^p_{vib} \; - \; \overline{\dot{R}}^p_{VT} \tag{6}$$

$$\frac{\partial \overline{\rho}\widetilde{Y_k}}{\partial t} + \frac{\partial (\overline{\rho}\widetilde{u_i}\widetilde{Y_k})}{\partial x_i} = \frac{\partial}{\partial x_i}\left(\left[F\Xi \frac{\overline{\mu}}{S_{c,k}} + (1-S)\frac{\mu_t}{S^t_{c,k}}\right]\frac{\partial \widetilde{Y_k}}{\partial x_i}\right) + \frac{\Xi}{F} W_k \overline{\dot{\omega}}^c_k \; + \; W_k \overline{\dot{\omega}}^p_k \tag{7}$$

where $\overline{\varphi}$ and $\widetilde{\varphi}$ are Reynolds and Favre filtering of variable φ. μ, S_c and P_r are the viscosity, the Schmidt and Prandtl numbers, respectively, where t superscript denotes for turbulent quantities. The dynamical formulation of the thickening factor reads $F = 1 + (F_{\max} - 1)S$, where the flame sensor S equals 0 and 1 outside an inside the reactive layer, respectively. Ξ is the sub-grid scale flame wrinkling. $\overline{\dot{\omega}}^c_k$, the chemical reaction rate due to combustion, is modeled by a detailed mechanism. $\overline{\dot{\omega}}^p_k$, the filtered chemical reaction rate due to plasma chemistry is modeled by assuming that the dissociation of O_2 into O dominates:

$$\overline{\dot{\omega}}^p_O = \eta \, \frac{\widetilde{Y}_{O_2}}{Y^f_{O_2}} \, \frac{\dot{E}^p}{e_O \, W_O} \tag{8}$$

$$\overline{\dot{\omega}}^p_{O2} = -\frac{W_O}{W_{O2}} \, \overline{\dot{\omega}}^p_O \tag{9}$$

$$\overline{\dot{\omega}}^p_k = 0 \quad \text{if k} \neq O_2, O \tag{10}$$

As the plasma chemistry are much faster than flow time scales, sub-grid scale interactions between turbulence and plasma have been neglected. The term $\dot{R}^p_{VT}$ in both Eq. (5) and Eq. (6) refers to the relaxation rate of the vibrational energy into gas heating and is closed using a Landau-Teller harmonic oscillator as indicated in [18].

The filtered rate of energy, $\overline{\dot{E}}^p_{chem}$,$\overline{\dot{E}}^p_{heat}$ and $\overline{\dot{E}}^p_{vib}$ are closed from Eq. (2), Eq. (3) and Eq. (4) by neglecting sub-grid scale contribution, i.e. by assuming that $\overline{\dot{E}}^p_y = \dot{E}^p_y(\widetilde{Y}_{O_2}, \overline{\dot{E}}^p)$.

3. MiniPAC configuration

3.1. Experimental set-up

The MiniPAC configuration is a premixed methane-air bluff-body stabilized turbulent flame. The 200-mm-length injection tube has an inner diameter of 16 mm and the bluff-body diameter is 10 mm. Nanosecond discharges are produced downstream of the bluff-body between a horizontal tungsten anode of 1 mm diameter centered 5 mm above the grounded cathode which consists of a 2 mm height, 1 mm diameter pin inserted in the middle of the bluff-body.

The burner is fed with a methane-air mixture ($\phi = 0.8$), injected at a constant volumetric flow rate $\dot{m} = 17.4\ m^3\ h^{-1}$ which corresponds to a bulk velocity of $U_b = 43.3$ m.s^{-1} and a Reynolds number of $Re = 1.6\ 10^4$.

The discharges properties have been experimentally characterized [21]. They have a quasi-cylindrical shape of 5 mm length corresponding to the inter-electrode distance, and a radius equal to 1.0 mm, a pulse energy of 2 mJ deposited in 50 ns and repeated at a frequency of 20 kHz. Photographies of non-assisted and plasma-assisted flames are shown in Fig. 2. Without discharge (left), a weak and incomplete combustion is restricted to the bluff-body wake. However, the application of NRP discharges allows the flame enhancement and stabilization (right).

Fig. 2: Photographs of the lean flame (ϕ = 0.8) without (left) and with (right) NRP discharges applied at 20 kHz. Figure extracted from [21]

3.2. Numerical set up

LES of the MiniPAC stabilization by NRP discharges are performed using the YALES2 unstructured finite-volume low-Mach number solver [22]. The time integration is performed using a fourth-order temporal scheme with a centred fourth order scheme for spatial discretization. The sub-grid Reynolds stresses tensor is closed using the Dynamic Smagorinsky model [23]. The analytical LU19 kinetic scheme involving 19 species and 184 reactions is used for the methane-air mixture chemistry [24], species equations are coupled with turbulence using the Thickened Flame model for LES (TFLES) [20] and the Charlette sub-grid scale flame wrinkling model [25]. The mesh consists of 140 millions tetrahedral elements refined in the plasma discharge zone, with a cells size equals 0.1 mm, to ensure that the small turbulence scales and laminar flame thickness are well resolved and no sub-grid scale model or TFLES coupling is necessary [18]. In the flame area, the cells size varies from 0.1 mm to 0.2 mm. The TFLES model is used in this region to capture the turbulence-flame interaction, triggered by a dynamic sensor.

The discharge properties have been set to be consistent with experimental measurements. It has a cylindrical shape filtered with the spatial function $F(r) = erfc[(r/a)^b]$ where r is the radial distance from the discharge axis. a and b are geometric parameters, fitted to well reproduce the discharge radius and have a sufficient number of point at discharge interface to avoid high gradients that can cause numerical issues.

A reactive LES is first conducted without NRP discharges until reaching a steady-state solution. Then, from the same initial condition,which define t=0, two LES are performed: one still without activating plasma (case NP) and a second one with applying an uninterrupted series of NRP discharges in the burnt gases of the flame above the bluff-body at a frequency of 20kHz (case P).

Figure 3 shows the 2D mean axial velocity on the centerline plane obtained from case NP. An inner recirculation zone is clearly identified behind the bluff-body. The same analysis conducted on case P shows that the shape and the size of the recirculation are not significantly affected by the electric discharges.

4. Analysis of the plasma-assisted combustion mechanism

Quantitative comparisons between experiments and simulations have been performed to validate the modeling approach consistency. The comparisons of the gas temperature evolution at the center of the discharge in [21] and OH profile along the line passing through the center of the discharge (4.5 mm above the bluff body) [26] during the pulsing sequence show a very good agreement between the experiment and the numerical simulation with less than 10% difference when steady state is reached. The local effects of the NRP discharges applied on lean burnt gases are well capture by the model.

Global scale comparisons have also been performed.The direct experimental visualization of the OH* chemiluminescence against the simulated OH mass fraction conducted by Blanchard *et al.* [21]

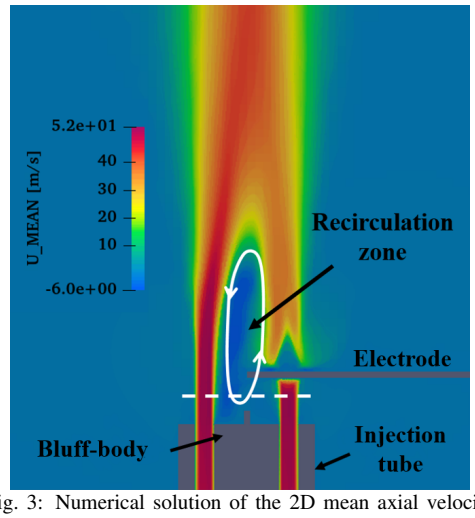

Fig. 3: Numerical solution of the 2D mean axial velocity on the centerline plane of the Mini-PAC configuration (case NP). The burner geometry and the positions of the electrodes are indicated. The dashed white line shows the position of radial profiles analyzed in section 4.

show that the influence of plasma on the flame shape and length is also well predicted by the LES.

To understand the local and global interaction mechanisms between the plasma and the flame involved in plasma-assisted flame enhancement process a detailed numerical analysis is performed.

4.1. Global impact of NRP discharges

The global impact of NRP discharges on the total heat release is evidenced in Fig. 4, which plots the temporal evolution of the thermal flame power $P = \int_V (\Xi/F)\overline{\dot{\omega}}_H dV$, where $\overline{\dot{\omega}}_H$ is the filtered heat release rate and $\int_V$ denotes the volumetric integral over the whole computational domain V. Without NRP discharges, the flame power oscillates around 700 W. However, when the electrical discharges are turned on, the total heat released by the combustion increases gradually during a transient period of approximately 10 ms (200 pulses) and then oscillates around a value of 1600 W.

To identify the reasons of the flame power increase, the LES-resolved $\mathcal{R}$ and total $\mathcal{A}$ flame surfaces are computed as [27]:

$$\mathcal{R} = \int_V \overline{|\nabla c|} dV \quad \text{and} \quad \mathcal{A} = \int_V \Xi \overline{|\nabla c|} dV \quad (11)$$

where c is a progress variable defined from the temperature to reach 0 and 1 in the fresh and burnt gases, respectively. Two observations are made from the analysis of the temporal evolution of $\mathcal{R}$ and $\mathcal{A}$ plotted in Fig. 5. First, $\mathcal{R}$ is very close to $\mathcal{A}$ and in practice 95% of the flame wrinkling is resolved at the LES scale. The grid resolution is here sufficiently fine to limit turbulent combustion modeling errors. Second,

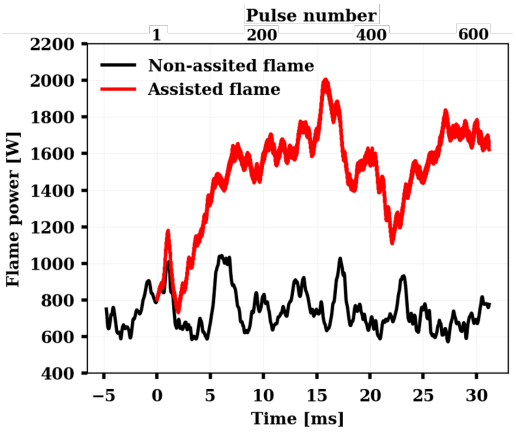

Fig. 4: Temporal evolution of the total thermal flame power for cases NP (black) and P (red).

the flame surface evolution follows the same trend than the flame power plotted in Fig. 4.

The mean gains in power (η_P) and total flame surface ($\eta_\mathcal{A}$) induced by the NRP discharges are defined as:

$$\eta_P = \langle P_P \rangle / \langle P_{NP} \rangle \quad \text{and} \quad \eta_\mathcal{A} = \langle \mathcal{A}_P \rangle / \langle \mathcal{A}_{NP} \rangle \quad (12)$$

where $\langle \varphi \rangle$ denotes temporal averaging of variable φ. P and NP subscripts refer to simulations with and without plasma, respectively. To remove the transient state following by the discharges activation, the mean gains are computed for the period [7ms,20ms]. It comes that $\eta_P = 2.13$ and $\eta_\mathcal{A} = 1.54$. The ratio $\eta_\mathcal{A}/\eta_P = 0.72$, which means that approximately 70 % of the gain in flame power is explained by an increase of the total flame surface. As it will be shown further, the rest of the gain (30%) is explained by a local increase of the heat release (and the flame consumption speed) in the periphery of the bluff-body recirculation zone.

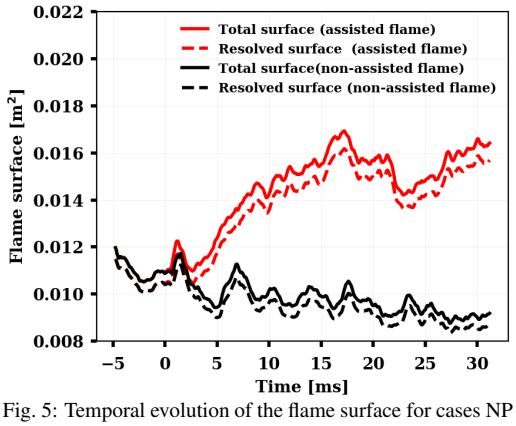

Fig. 5: Temporal evolution of the flame surface for cases NP (black) and P (red). Dashed lines represent the flame surface resolved at the LES filter scale, while solid lines include also the subgrid flame wrinkling contribution.

4.2. Impact of NRP discharges on the heat release field

Figure 6 shows two instantaneous snapshots from cases NP (left) and P (right), taken at the same time instant t= 20 ms, of the flame surface (defined as the iso-surface of $c^* = 0.5$) colored by the heat release. Without NRP discharges, only a weak reaction zone limited to the recirculation zone behind the bluff body is visible. Indeed, because of the low burning velocity under lean conditions, the flame front cannot propagate outside the recirculation zone. Figure 6 (right) plots the flame surface after 400 pulses. In comparison with case NP, the heat released by the flame increased significantly and the reaction zone extended downstream. As expected from the previous global analysis, the flame surface is developed. The pulsation of the electrical discharges enables the recirculation zone to act as a flame holder. A chemical analysis is conducted to understand how the NRP discharges, located at the center of the bluff-body, will attach the flame around the recirculation zone.

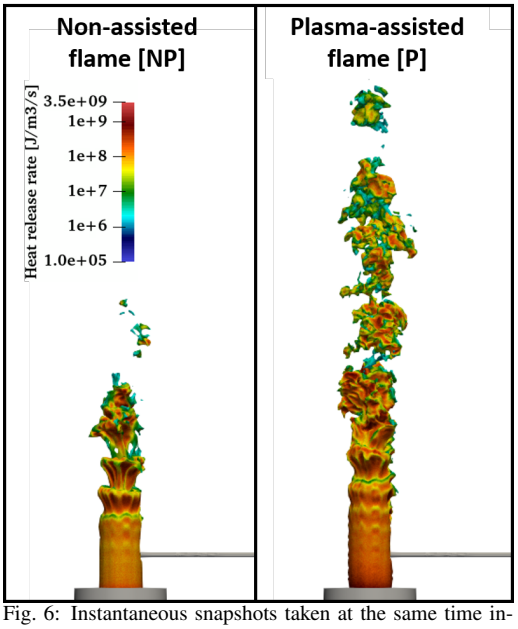

Fig. 6: Instantaneous snapshots taken at the same time instant t= 20 ms of $c^* = 0.5$ iso-surface colored by the heat release for cases NP (left) and P (right).

4.3. Chemical influence of NRP discharges in the recirculation zone

Average thermo-chemical quantities are computed over the period [10ms,20ms], for both cases NP and P. Radial profiles then are extracted at the position indicated in Fig. 3, located 4.5 mm above the bluff body, which crosses both the center of the discharges and the bluff-body recirculation zone. Mean radial heat release and methane consumption rates are plotted in Figs. 7 (top) and (bottom), respectively. The peak of heat release observed in both NP and P cases corresponds to the flame reactive layer, whose position was also evidenced in Fig. 6. The application of NRP discharges at the center of the bluff-body (x=0) causes a significant increase of heat release rate in the reactive layer located at 4 mm $<$ r $<$ 5 mm, which is accompanied by an increase of the methane consumption. The methane source term and the heat release rate are affected by the same factor (≈2.2), which means that the increase of the heat release rate is directly related to the increase of the methane consumption when NRP discharges are applied.

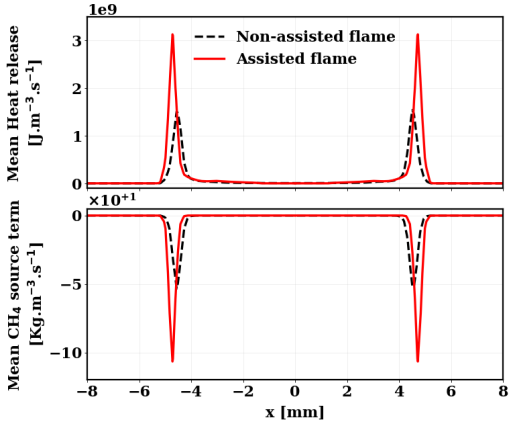

Fig. 7: Comparison of mean flame heat release rate (top) and mean CH_4 source term (bottom) radial profiles 4.5 mm above the bluff body for cases NP (dashed black line) and P (red line).

Figure 8 shows the mean radial profile of temperature across the recirculation zone. For case NP, the temperature of the burnt gases contained within the recirculation zone is around 1950K which corresponds to the adiabatic flame temperature of a methane-air mixture at an equivalence ratio of 0.8. However, for the plasma-assisted flame, the mean temperature increases up to 3500K in the plasma zone, where the thermal energy is deposited. This energy is convected by the flow from the center to the periphery of the recirculation zone and induces a temperature increase in the flame front, i.e. at 4 mm $<$ r $<$ 5 mm.

Figures 9 and 10 plot the mass fraction of species H_2O-CO_2-O_2-CO and OH-O-H_2-H, repectively. Without plasma, the chemical composition within the recirculation zone corresponds to thermo-chemical equilibrium condition of the methane-air mixture with equivalence ratio of 0.8. When plasma is activated, both H_2O and CO_2 are highly consumed in the discharge zone. At the opposite, the mass fractions of the other species, in particular O and OH, increases significantly.

Figure 11 (left) and (right) shows the chemical pathway diagram in the plasma region during and after a pulse, respectively. The thickness of the arrow is proportional to the reaction rates integrated within

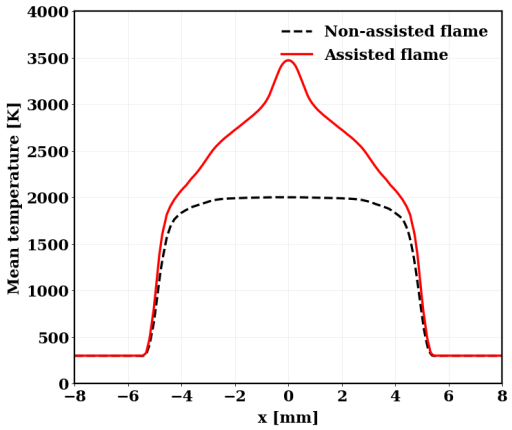

Fig. 8: Comparison of mean temperature at 4.5 mm above the bluff body for cases NP (dashed black line) and P (red line).

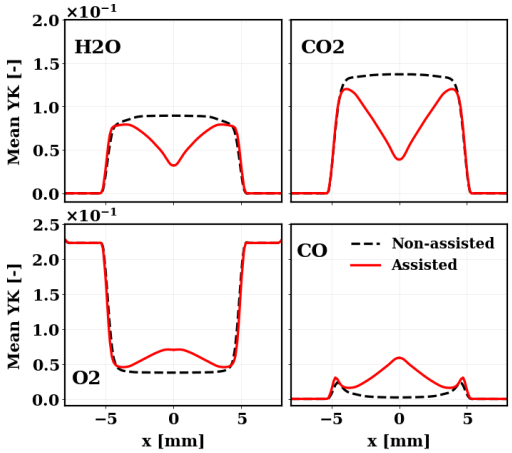

Fig. 9: Comparison of mean species mass fractions (H_2O, CO_2, O_2, CO) at 4.5 mm above the bluff body for cases NP (dashed black line) and P (red line).

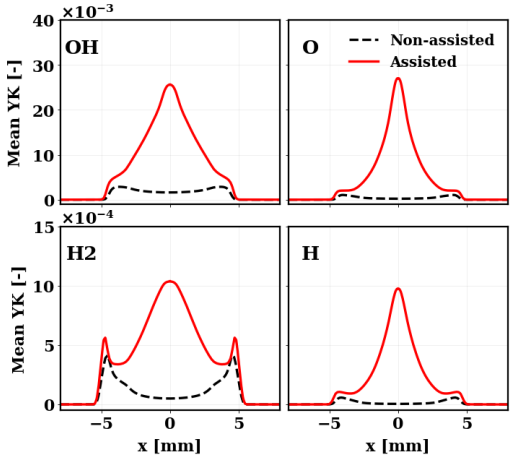

Fig. 10: Comparison of mean species mass fractions (OH, O, H_2, H) at 4.5 mm above the bluff body for cases NP (dashed black line) and P (red line).

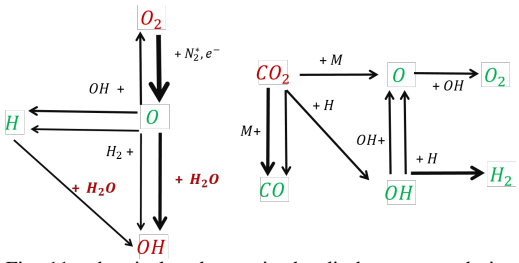

Fig. 11: chemical pathways in the discharge zone during (left) and after (right) a pulse.

the discharge zone. As discussed in [12, 16], O_2 is mainly dissociated into O atoms during an electric pulse (Fig. 11 (left)), by the relaxation of nitrogen electronic state. The, the atomic oxygen produced by the discharge reacts with H_2O contained in the burnt gases to produce OH and H. As shown in Figure 11 (right), chemical pathways are completely different after the pulse. CO_2, the main reactant, is consumed by heat and radicals produced during the pulse, leading to a production of CO, H_2, O_2, O and OH. Fig. 9 and 10 show that, among the species produced in the discharge zone, those with a long lifespan such as OH, O_2 and H_2 are convected up to the flame front in large quantities. At the opposite, species with a shorter lifespan such as O, H does not survive outside the discharge zone.

A second chemical analysis, shown in Fig. 12, is performed in the flame reactive layer (4 mm $<$ r $<$ 5 mm) front to identify the CH_4 consumption pathways without and with NRP discharges. Without plasma, CH_4 is mainly consumed by OH, H and O trough the following three elementary reactions:

$$CH_4 + OH \rightarrow CH_3 + H_2O \qquad (R_1)$$
$$CH_4 + H \rightarrow CH_3 + H_2 \qquad (R_2)$$
$$CH_4 + O \rightarrow CH_3 + OH \qquad (R_3)$$

The impact of the plasma on the rate of progress of reactions R_1, R_2 and R_3 is indicated in Fig. 12. As discussed previously, NRP discharges supply the reaction zone with OH, H_2 and O_2. The increase of OH concentration will enhance directly the reaction R_1 by 51%. H_2 and O_2 are dissociated into H and O radicals in the flame reaction zone, increasing therefore also the rate of reactions R_2 and R_3 by 27% and 21%, respectively.

In conclusion, the discharges produces heat and species (OH,H_2,O_2), which are convected within the recirculation zone. Because of its longer lifespan, OH is the main plasma-induced species that reaches the flame front and enhance significantly the chemical reactivity at the flame basis surrounding the recirculation zone. Such local increase of the reactivity enhances the heat release in the periphery of the recirculation zone but also acts as a flame-holder which enables the turbulent flame surface development, increasing the total combustion efficiency.

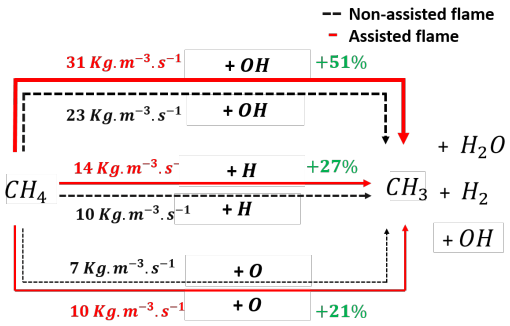

Fig. 12: CH4 consumption pathways in the flame front without NRP discharges (dashed black line) and with NRP discharges (red line).

The results of the analysis are consistent with the experimental images in [28] that show an enhancement of the flame when the OH produced by the discharge reaches the flame front.

5. Conclusion

The numerical analysis of Large Eddy Simulation of the Mini-PAC burner concludes to the following mechanisms of turbulent premixed flame stabilization by nanosecond repetitively pulsed (NRP) discharges:

1. The electrical pulses generate a plasma in the discharge zone, which produces O atom and heat.
2. During the pulse, O reacts with H_2O to form mainly OH, through the reaction O+ $H_2O \rightarrow$ 2OH. After the pulse, CO_2 reacts in the inter-electrode region to form H_2 and O_2.
3. Because of their long lifespan, OH, H_2 and O_2 are the main plasma-induced species convected to the flame front thanks to the bluff-body recirculation zone.
4. OH, H_2 and O_2 are consumed with CH_4 in the flame reactive layer surrounding the recirculation zone and locally increase the flame heat release rate. This local increase of the heat release in the vicinity of the recirculation zone is responsible of 30% of the gain in flame power induced by the plasma.
5. The local increase of heat release rate anchored the turbulent flame front which can develop downstream.
6. The total flame surface is increased, increasing the combustion efficiency by 70%.

This analysis is based on the assumption that O_2 dissociation is the key chemical effect of plasma on combustion chemistry. Future works will aim to challenge this hypothesis by extending the plasma combustion model to account for the dissociation of other species present in the recirculating burnt gases, such as CO_2 and H_2O dissociation induced by the discharge plasma chemistry.

Acknowledgments

This work was supported by the ANR programs PASTEC (ANR-16-CE22-0005-01) and granted access to the HPC resources from IDRIS, TGCC and CINES under the allocation A0052B10253 made by GENCI (Grand Equipement National de Calcul Intensif) and HPC resources from the Mesocentre computing center of CentraleSupelec and Ecole Normale Superieure Paris-Saclay supported by CNRS and Région Ile-de-France (http:// mesocentre.centralesupelec.fr/).We acknowledge PRACE for awarding us access to Joliot-Curie at GENCI@CEA, France. Victorien Blanchard, Nicolas Minesi and Christophe Laux from EM2C lab are acknowledged for providing the experimental data.Vincent Moureau and Ghislain Lartigue from CORIA lab are acknowledged for providing the YALES2 code.

References

[1] S. Candel, Combustion dynamics and control: Progress and challenges, Proc. Combust. Inst. 29 (1) (2002) 1–28.

[2] K. Criner, A. Cessou, J. Louiche, P. Vervisch, Stabilisation of turbulent lifted jet flame assisted by pulsed high voltage discharge, Combust. Flame 144 (2006) 422–425.

[3] W. Kim, H. Do, M. G. Mungal, M. A. Cappelli, Flame stabilisation enhancement and nox production using ultra short repetitively pulsed plasma discharges, In 44th AIAA Aerospaee Sciences Meeting and Exhibit Reno, NV USA, 2006.

[4] S. M. Starikovskaia, Plasma assisted ignition and combustion, Journal of Physics D: Applied Physics 39 (16) (2006) R265–R299.

[5] Y. Ju, W. Sun, Plasma assisted combustion: dynamics and chemistry, Prog. Energy Sci. Combust. 48 (2015) 21–83.

[6] G. Pilla, Etude experimentale de la stabilisation de flammes propane-air de pre-melange par decharges nanosecondes impulsionnelles repetitives., Ph.D. thesis, Ecole Centrale Paris, France, 2008.

[7] M. S. Bak, S. K. Im, M. G. Mungal, M. A. Cappelli, Studies on the stability limit extension of premixed and jet diffusion flames of methane, ethane, and propane using nanosecond repetitive pulsed discharge plasmas, Combust. Flame 160 (2013) 2396–2403.

[8] S. Barbosa, G.Pilla, D. Lacoste, P.Scouflaire, S. Ducruix, C. Laux, D. Veynante., Influence of nanosecond repetitively pulsed discharges on the stability of a swirled propane/air burner representative of an aeronautical combustor, Phil. Trans. R. Soc. A. 373 (2015).

[9] G. Vignat, N. Minesi, P. R. Soundararajan, D. Durox, A. Renaud, V. Blanchard, C. O. Laux, S. Candel, Improvement of lean blow out performance of spray and premixed swirled flames using nanosecond repetitively pulsed discharges, Proc. Combust. Inst. 38 (4) (2021) 6559–6566.

[10] F. D. Sabatino, D. A. Lacoste, Enhancement of the lean stability and blow-off limits of methane-air swirl flames at elevated pressures by nanosecond repetitively pulsed discharges, J. Phys. D: Appl. Phys. 53 355201 (2020).

[11] F. D. Sabatino, T. F. Guiberti1, J. P. Moeck, W. L. Roberts, D. A. Lacoste, Actuation efficiency of nanosecond repetitively pulsed discharges for plasma-assisted swirl flames at pressures up to 3 bar, J. Phys. D: Appl. Phys. 54 075208 (2021).

[12] D. L. Rusterholtz, D. A. Lacoste, G. D. Stancu, D. Z. Pai, C. O. Laux, Ultrafast heating and oxygen dissociation in atmospheric pressure air by nanosecond repetitively pulsed discharges, Journal of Physics D: Applied Physics 46 464010 (2013) (p. 14, 18, 39, 49, 50, 52, 56, 57, 62, 68, 71, 74, 79).

[13] N. A. Popov, Fast gas heating initiated by pulsed nanosecond discharge in atmospheric pressure air., AIAA Aerospace Sciences Meeting, Grapevine, TX, 2013.

[14] M. S. Bak, H. Dob, M. G. Mungal, C. M. A, Plasma-assisted stabilization of laminar premixed methane/air flames around the lean flammability limit, Combust. Flame 159 (2012) 3128–3137.

[15] F. Tholin, D. A. Lacoste, A. Bourdon, Influence of fast-heating processes and o atom production by a nanosecond spark discharge on the ignition of a lean h2–air premixed flame, Combust. Flame 161 (5) (2014) 1235–1246.

[16] M. M.Castela, B. Fiorina, A. Coussement, O. Gicquel, N. Darabiha, C. O. Laux, Modelling the impact of non-equilibrium discharges on reactive mixtures for simulations of plasma-assisted ignition in turbulent flows, Combust. Flame 166 (2016) 133–147.

[17] M. Castela, B. Fiorina, S. Stepanyan, A. Coussement, O. Gicquel, N. Darabiha, C. Laux, A 3-d dns and experimental study of the effect of the recirculating flow pattern inside a reactive kernel produced by nanosecond plasma discharges in a methane-air mixture, Proc. Combust. Inst. 36 (2017) 4095–4103.

[18] Y. Bechane, B. Fiorina, Numerical investigations of turbulent premixed flame ignition by a series of nanosecond repetitively pulsed discharges, Proc. Combust. Inst. 38 (4) (2021) 6575–6582.

[19] N. Q. Minesi, V. P. Blanchard, E. Pannier, G. D. Stancu, C. O. Laux, Plasma-assisted combustion with nanosecond discharges. i: Discharge effects characterization in the burnt gases of a lean flame plasma, Sources Sci. Technol. 31 045029 (2022).

[20] O. Colin, F. Ducros, D. Veynante, T. Poinsot, A thickened flame model for large eddy simulations of turbulent premixed combustion, Physics of Fluids 12, 1843.

[21] V. Blanchard, N. Q. Minesi, Y. Bechane, B. Fiorina, C. O. Laux, Experimental and numerical characterization of a lean turbulent premixed flame stabilized by nanosecond discharges, in: AIAA Scitech, 2021.

[22] V. Moureau, P. Domingo, L. Vervisch, Design of a massively parallel cfd code for complex geometries., Comptes Rendus Mécanique C. R. Mecanique 339 (2011) 141–148.

[23] M. Germano, U. Piomelli, P. Moin, W. Cabot, A dynamic subgrid-scale eddy viscosity model, Physics of Fluids A: Fluid Dynamics 3 (7) (1989) 1760–1765.

[24] T. Lu, L. C. K., A criterion based on computational singular perturbation for the identification of quasi steady state species: a reduced mechanism for methane oxidation with no chemistry, Combust. Flame 154 (4) (2008) 761–774.

[25] F. Charlette, D. Veynante, C. Meneveau, A power-law wrinkling model for les of premixed turbulent combustion: Part i non dynamic formulation and initial tests, Combust. Flame 131 (2002) 159–180.

[26] N. Minesi, Thermal spark formation and plasma-assisted combustion by nanosecond repetitive discharges, Ph.D. thesis, Université Paris-Saclay, France 2020, (p. 174-175).

[27] D. Veynante, L. Vervisch, Turbulent combustion modeling, Progress in Energy and Combustion Science 28 (3) (2002) 193–266.

[28] D. Xu, Thermal and hydrodynamic effects of nanosecond discharges in air and application to plasma-assisted combustion, Ph.D. thesis, Ecole Centrale Paris, France 2013, (p. 106-108).